



Article

Full-Cut Manufacture of Skin-Interfaced Microfluidic Patch with Copper Electrode for In Situ Admittance Sensing of Sweat Rate

Lei Wei ^{1,2,†}, Yuxin He ^{1,†}, Zihan Lv ¹, Daoyou Guo ¹, Lin Cheng ¹, Huaping Wu ³ and Aiping Liu ^{1,*}¹ Key Laboratory of Optical Field Manipulation of Zhejiang Province, Zhejiang Sci-Tech University, Hangzhou 310018, China² School of Physics and Electronics Engineering, Fuyang Normal University, Fuyang 236037, China³ Key Laboratory of Special Purpose Equipment and Advanced Processing Technology, Ministry of Education and Zhejiang Province, College of Mechanical Engineering, Zhejiang University of Technology, Hangzhou 310023, China

* Correspondence: liuaiping1979@gmail.com

† These authors contributed equally to this work.

Abstract: Sweat-rate measurement has received more and more attention, especially for specific groups, such as athletes, soldiers and manual workers, due to their excessive sweat loss under prolonged intense heat stress, which increases the risk of dehydration and electrolyte imbalance. The highly effective manufacture of a sweat-sensing device is essential to its wide range of applications in perspiration-related physiological information detection. In this work, we propose a simple and cost-effective strategy for the manufacture of a microfluidic sweat-rate-sensing patch via laser cutting and transfer printing technology. A copper foil tape is used as the electrode for in situ admittance based sweat-rate-sensing. The detection circuits and measurement conditions are optimized to prevent the negative effect of an electrochemical reaction between a copper electrode and sweat for precise admittance measurement. In vitro and on-body experiments demonstrate that the copper electrode is applicable for admittance-based sweat sensing and is capable of achieving equivalent sensing accuracy as a gold electrode and that the proposed sensor structure can perform consecutive and accurate sweat-rate-sensing and facilitates a significant increase in manufacturing efficiency.



Citation: Wei, L.; He, Y.; Lv, Z.; Guo, D.; Cheng, L.; Wu, H.; Liu, A.

Full-Cut Manufacture of Skin-Interfaced Microfluidic Patch with Copper Electrode for In Situ Admittance Sensing of Sweat Rate. *Biosensors* **2023**, *13*, 67. <https://doi.org/10.3390/bios13010067>

Received: 1 December 2022

Revised: 28 December 2022

Accepted: 30 December 2022

Published: 31 December 2022



Copyright: © 2022 by the authors. Licensee MDPI, Basel, Switzerland. This article is an open access article distributed under the terms and conditions of the Creative Commons Attribution (CC BY) license (<https://creativecommons.org/licenses/by/4.0/>).

Keywords: sweat rate; microfluidic patch; copper electrode; laser cutting; admittance

1. Introduction

Perspiration is a crucial role in the thermoregulation of the body. For specific groups, such as athletes, soldiers and manual workers, excessive sweat loss under prolonged intense heat stress may increase the risk of dehydration and electrolyte imbalance, which can degrade individuals' physical performances, compromise their physiological status, and even develop into fatal heat-related illnesses [1,2]. Measurement of sweat rate is helpful to provide a reasonable guidance for fluid intake [3,4] to ensure water and electrolyte balance in vivo. Recently, colorimetric [5–10], volumetric [11,12], calorimetric [13], capacitive [14,15], and impedance (or admittance) [16–21] sensing methods have been developed for the in situ measurement of sweat rate, but several challenges remain, such as inconvenience in automatic monitoring [5–9,11], requiring precise alignment in the micromachining process [13,16–18], and the required pre-calibration [17]. Besides, the vacuum-evaporated gold electrode commonly used for sweat rates requires time-consuming, multistep micromachining processes and increases manufacturing costs accordingly. [16,17,20,22]. In contrast, a copper electrode is a simple and low-cost alternative, especially in small-batch production, and it has been used in water oxidation reaction and CO₂ electroreduction [23,24]. However, when the copper electrode is immersed in sweat, the electrochemical reactions at the Cu/sweat interface may occur and lead to the dissolution of the copper electrode [25] or

the generation of bubbles, which will seriously affect the measurement accuracy. In order to avoid the occurrence of electrochemical reactions, a non-contact measurement method for sweat rate based on the copper capacitive sensor was designed, but only a weak output signal could be obtained [14]. However, the acquisition of a strong, stable and veritable test signal of sweat rate based on the copper electrode sweat sensing remains challenging.

Herein, we report a microfluidic patch with a copper electrode to measure the sweat rate by calculating the increasing rate of the measured admittance of the electrode in a microchannel when sweat advanced in the microchannel. The electrode admittance was measured by detection circuits that were optimized to prevent the negative effect of the electrochemical reaction in contacting admittance measurement, namely filtering the DC component of the excitation signal passing through the sensor to avoid the DC polarization of the electrodes, setting the highest frequency and the lowest amplitude of the excitation signal to minimize the influence of the electrochemical reaction on admittance measurement. Furthermore, the special structural design of electrodes in the microchannel and the use of copper foil as electrode material enable the rapid manufacture of the entire microfluidic patch using only laser cutting and rapid transfer printing technologies without precise alignment operation, surface treatment or modification of electrodes. The proposed easy-to-manufacture and low-cost microfluidic patch is capable of outputting a strong and credible admittance signal. In vitro and on-body experiments together demonstrated the validity of using copper electrodes and verified the accuracy of the proposed microfluidic patch for sweat-rate measurement.

2. Materials and Methods

2.1. Structure Design of the Microfluidic Patch

The microfluidic patch for sweat-rate measurement consists of three parts, namely detection area, calibration area (for sweat-rate calibration), and electrical interface, as illustrated in Figure 1a. The detection area and calibration area are constituted by a stacking microchannel layer and a copper electrode layer consisting of two pairs of parallel electrodes (Figure 1b). Only a small part of each electrode is located inside the microchannel, and every pair of the electrodes is separated by a distance of 200 μm (Figure 1a and Figure S1). Two PET films encapsulate the electrode layer and the microchannel layer. The microfluidic patch can be attached to the skin via a double-sided adhesive layer with a 5 mm hole for dynamic sweat sampling (Figure 1b). Collected sweat first flows into the 7.5 mm calibration area, then passes through it and enters the detection area. Newly-arrived sweat in the detection area increases the electrode admittance whose increment rate depends on the sweat rate and electrolyte concentration. The calibration area can decode the electrolyte concentration that is used to calibrate the sweat rate measured from the admittance of the detection area.

Based on the structure design above, the electrodes and microchannel can be conveniently fabricated by laser cutting, respectively following the corresponding cutting tracks shown in Figure 1c. Thus there is no need to embed two parallel copper electrodes into the microchannel by precise alignment operation, which can significantly improve manufacturing efficiency and product consistency. The patch integrated with a flexible printed circuit board (FPCB) can be easily mounted on the skin for in situ sweat collection and detection (Figure 1d).

It is important to note that, for sweat-rate measurement devices, the additional flow resistance of the device may affect the accuracy of sweat-rate detection. This is due to sweat being generated at the secretion coil of the eccrine gland and transported to the skin surface via the dermal duct and the upper coiled duct of the gland driven by secretory pressure [26,27], and the flow resistance of the gland and the secretory pressure determine the natural outflow rate of sweat from the sweat gland, which is the local sweat rate to be measured. However, a microfluidic sweat collection device inevitably increases the flow resistance in the sweat transport path. If the external flow resistance is large enough

to be close to the sweat gland's flow resistance, the sweat collection device will produce significant effect on the natural outflow rate of sweat from the sweat gland.

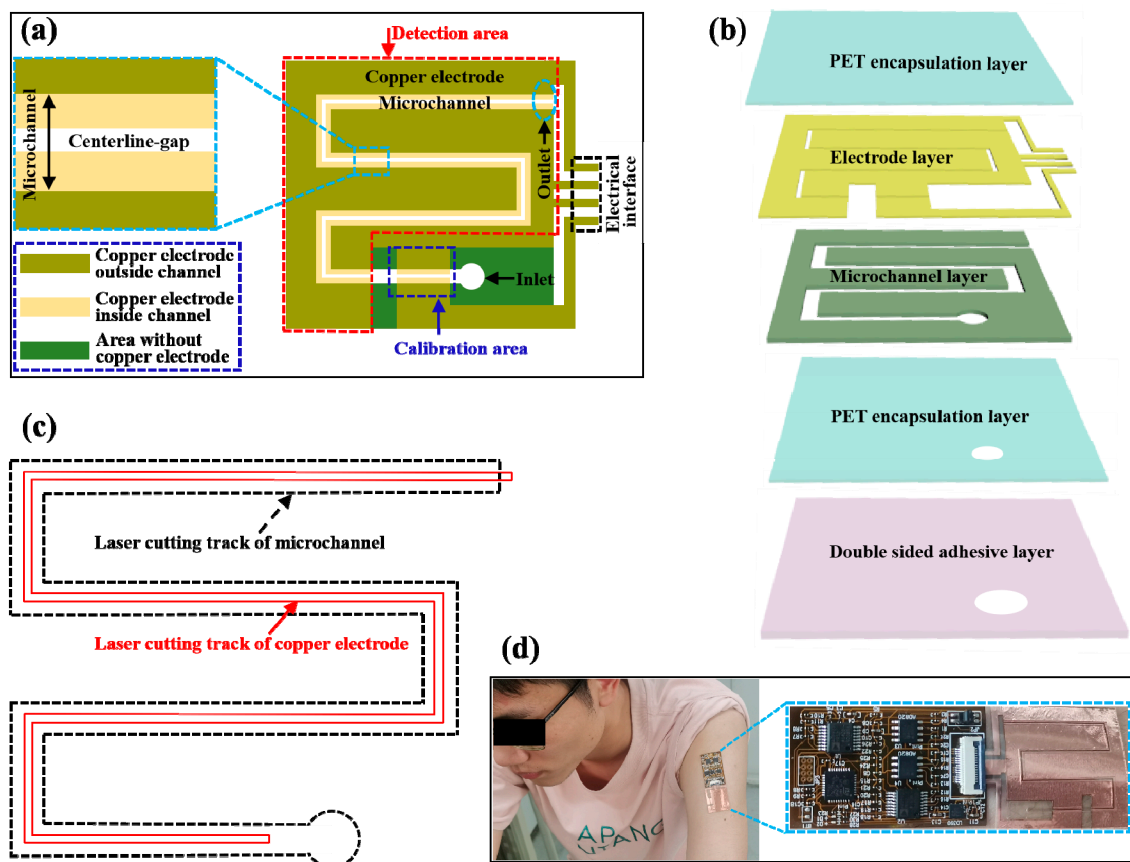


Figure 1. Design of microfluidic patch for sweat-rate sensing. (a) Structure of the microfluidic patch. (b) Exploded view of the patch. (c) Cutting tracks of microchannel and electrode. (d) Photograph of the patch integrated with FPCB mounted on the skin.

The flow of sweat in the microfluidic device is affected by both channel resistance and capillary pressure. Due to the small size of the microchannel, the microfluidic device may produce a considerable flow hindrance effect on sweat. In order to research the comprehensive impact of channel flow resistance and capillary pressure under a certain size of the microchannel, we study the equivalent flow resistance of the microchannel and obtain its formula as (more details refer to PART III of the Supplementary Materials):

$$R_{eq} = \frac{P_{gland}R_c + \Delta P_{\sigma}R_{gland}}{P_{gland} - \Delta P_{\sigma}} \quad (1)$$

where P_{gland} is the sweat-gland secretion pressure, ΔP_{σ} is the capillary pressure, R_c is the flow resistance of the microchannel, and R_{gland} is the flow resistance of the gland.

In this work, the microchannel is produced by laser-cutting acrylic double-sided tape and is packaged with PET film. The contact angle of sweat with the tape and the PET film are 100° [28] and 80.5° [29], respectively. The study reported in Reference [14] also used the same material for microchannel fabrication with a channel size of $90 \mu\text{m}$ in height, 1 mm in width and 350 mm in length. The equivalent flow resistance they provided was $4.6 \text{ kPa}\cdot\text{s}\cdot\text{mm}^{-3}$, consistent with the value of $4.68 \text{ kPa}\cdot\text{s}\cdot\text{mm}^{-3}$ calculated by Formula (1), demonstrating the validity of Formula (1). For the channel size in this work ($300 \mu\text{m}$ in height, 1 mm in width and 105 mm in length), the equivalent flow resistance of the microchannel is $0.31 \text{ kPa}\cdot\text{s}\cdot\text{mm}^{-3}$, far less than the flow resistance of the gland

(410 kPa·s·mm⁻³), so the designed microchannel device has little effect on the natural sweat secretion rate and sweat rate.

2.2. Principle of Admittance-Based Sweat-Rate Measurement via the Microfluidic Patch

Sweat contains a large amount of electrolytes, such as Na⁺, Cl⁻ and K⁺, which endow sweat with certain conductivity. When a certain volume of sweat fills the detection area of length dl during the time from t to $t + dt$ (Figure 2a), sweat and electrodes in this area of length dl will form a microcell whose equivalent circuit model is shown as Figure 2b, where C_d and R_{ct} represent the double-layer capacitance and charge-transfer resistance at the interface of the sweat-electrode, respectively. R_s is the solution resistance, and C_0 is the distributed capacitance between two parallel electrodes.

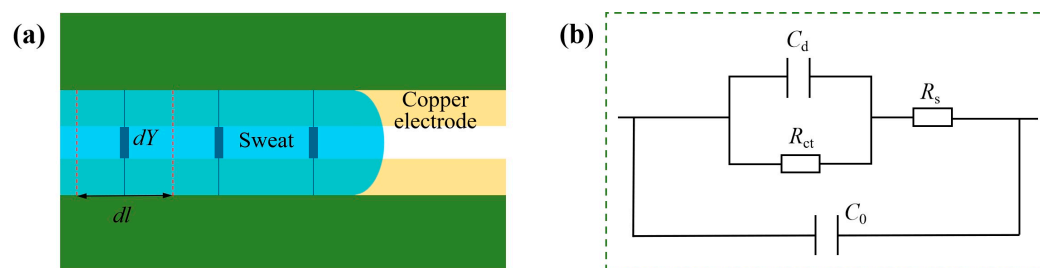


Figure 2. (a) Electrode admittance analysis model of sweat–electrode microsystem. (b) The equivalent circuit model of the microcell composed of electrodes and micro-sweat of length dl .

The equivalent circuit in Figure 2b can be further simplified as the admittance dY . Considering that flowing sweat in the microchannel can be regarded as a series of parallel admittances between two electrodes (Figure 2a), the electrode admittance increases with the increase in sweat volume in the microchannel. Furthermore, dY is related to the sweat electrolyte concentration, so the flow rate of sweat in the microchannel can be calculated by the formula:

$$Q_i = \frac{K}{c_i} \cdot \frac{Y_i - Y_j}{t_i - t_j} \quad (2)$$

where c_i , and Y_i are the sweat electrolyte concentration and the electrode admittance of the detection area at moment t_i , respectively, t_i and t_j are two adjacent sampling moments, and coefficient K is determined by both the microchannel size and the layout of electrodes in the channel. It is a constant for a specific sensor. The formula derivation refers to Part II of the Supplementary Materials.

2.3. Fabrication of Microfluidic Patch

A UV laser-cutter machine (ultraviolet laser-cutting machine-3W, Shenzhen Chaoyue Laser Intelligent Equipment Co., Ltd., ShenZhen, China) was used to fabricate all the layers of the microfluidic patch. The fabrication method and process are shown in Figure 3. First, the microchannel was fabricated by laser-cutting double-sided tape (9495LE 300LSE, 3M, Saint Paul, MN, USA) pasted on a silicone sheet pre-fixed on a countertop (Figure 3a) and then was peeled off the redundant area (Figure 3b). Then, copper foil tape (double conductive copper foil tape, Shenzhen Baojiasheng Adhesive Tape Products Factory, ShenZhen, China) was pasted onto the fixed microchannel layer and let its viscous surface be exposed (Figure 3c). After that, the UV laser was applied to cut copper foil along specific routes defined in the control software of the laser cutter machine (Figures 1c and 3d). After peeling off the removable copper foil, a centerline-gap appeared, which divided the copper foil tape into two electrodes (Figure S1 and Figure 3d). Then a PET film (12 μ m in thickness) was pasted on the adhesive surface of the copper foil to form strong interface adhesion between the PET film and the adhesive copper foil (Figure 3e). Thus, the microchannel and electrode layer could be transfer-printed onto the PET film by peeling them off together from the silicone sheet. With the help of the adhesion of the

copper foil tape, the aligned electrode and microchannel could be rapidly transfer-printed onto PET film without the thermal release tape or the water soluble tape, so it is efficient and low-cost when compared to previously reported transfer-printing strategies [30,31]. At last, the microchannel was completely encapsulated with another PET film to form the microchannel patch (Figure 3f). The prepared patch was further integrated with a FPCB for in situ sweat-rate sensing (Figure 1d).

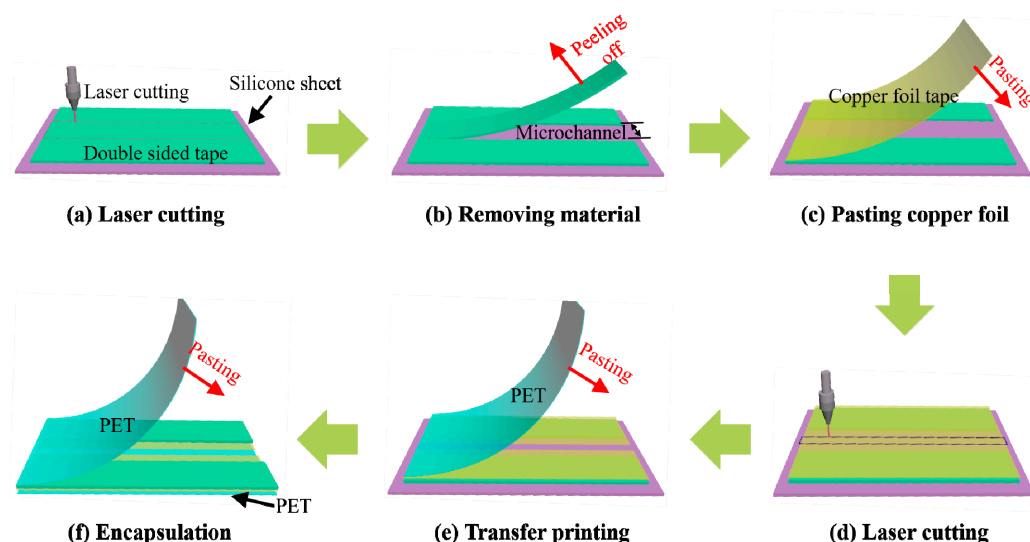


Figure 3. Fabrication process of microfluidic patch for admittance-based sensing of sweat rate.

2.4. Building Experimental Testing System

The in vitro characterization of the sensing performance of the microfluidic patch was carried out by a self-built injection analysis system as shown in Figure S2. In this system, a test solution was pumped into the microfluidic device by a syringe pump (LSP01-3A, Baoding Lange constant flow pump Co., Ltd., BaoDing, China). The injection scheme was designed as shown in Figure 4a. The test solution was injected into the sensor via an injection microchannel that was connected using a syringe with an amputated syringe needle and a flexible tube. Figure 4b shows the scheme for measuring the electrode admittance and transmitting it to a computer. Electrode admittance measurement was performed by AD5933-based circuits as shown in the dashed box, where a sinusoidal excitation signal was produced by the AD5933 chip. To minimize the influence of electrochemical reaction on admittance measurement, the highest frequency (100 kHz) and lowest amplitude (0.2 V) of the sinusoidal signal was set. Electrode polarization is a severe problem for admittance measurement, as it will generate microbubbles adsorbed on the electrode, which has a serious effect on the measurement results. So capacitance C2 was used to filter the DC component of the sinusoidal signal to avoid the DC polarization of the electrode. The design of the admittance measurement circuits in Figure 4b can completely avoid producing microbubbles and perform accurate admittance measurement based on the copper electrode. Detailed analysis about this is summarized in Part I of the Supplementary Materials. The real-time measured electrode admittance was read out by a microcontroller that was integrated on a FPCB together with AD5933-based admittance measurement circuits. In an in vitro characterization experiment, the acquired real-time admittance information was transferred to a computer via a data-transfer circuit, while in the on-body trial, the information was temporarily stored in the microcontroller and was transferred to the computer by the data-transfer circuits after the sweat induction trial.

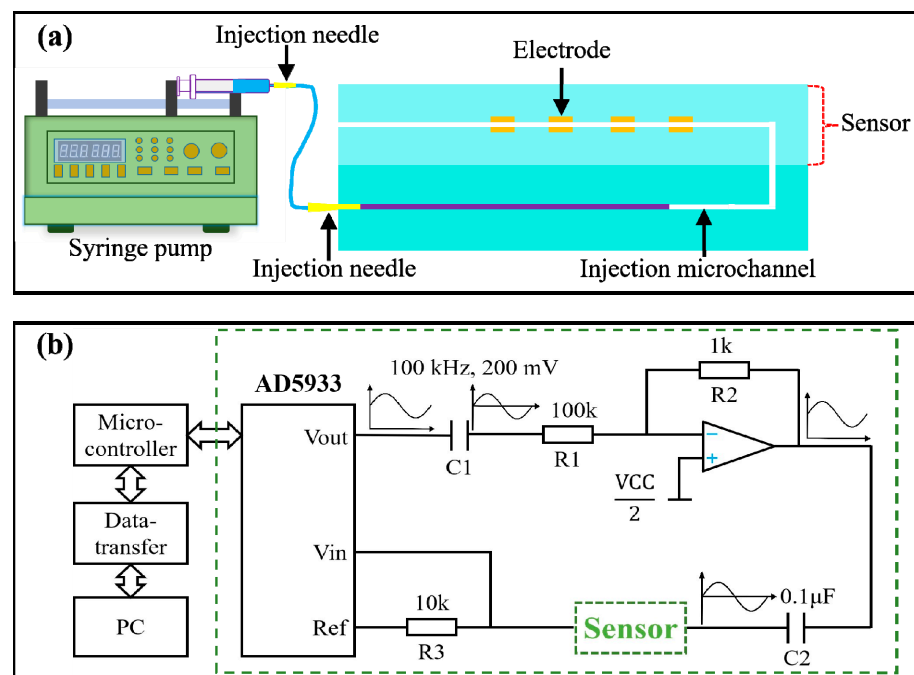


Figure 4. Schematic diagram of injection and measurement system. (a) Injection scheme of test solution in vitro experiments. (b) The schematic diagram of admittance measurement and data transmission.

3. Results and Discussion

3.1. Characterizing the Sensing Performance of Calibration Area

Since the sweat electrolyte concentration can affect the sweat-rate measurement, it should be simultaneously measured to calibrate the sweat rate according to Formula (2). In the calibration area, the model in Figure 2 can also be used to analyze the electrode admittance, which is only determined by the sweat electrolyte concentration when sweat completely saturates the electrode (referring to Part II of the Supplementary Materials). The sensing performance of the calibration area to the electrolyte concentration was characterized when NaCl solutions with different concentrations were injected into this area at the same rate of $2 \mu\text{L} \cdot \text{min}^{-1}$. As displayed in Figure 5a, the measured electrode admittances stayed constant in the same NaCl concentration and increased with the NaCl concentration increasing. An approximate proportional relationship between the electrode admittance and the NaCl solution concentration was obtained (Figure 5b), which demonstrates that the conductance is dominant in the admittance measurement of the solution-electrode system. This is the key reason why copper electrodes can perform the measurement of sweat electrolyte concentration. X-ray diffraction (XRD) characterization was used to investigate whether the copper electrode was corroded during the experiment. The three electrode samples, respectively, were the untreated copper electrode, a copper electrode soaked in NaCl solution for 1 hour and saved for 1 week, and the electrode taken from the microfluidic patch that was used for the on-body trial, respectively. The characterization results of the XRD of the three copper electrodes are shown in Figure 5c, and the results reveal that there is no production of new substances after soaking and on-body measurement. It is due to that the electrochemical transition between Cu atoms and Cu^{2+} is reversible and periodical when the excitation signal applied to the electrode is high-frequency sinusoidal AC voltage without the DC component. To further investigate the effect of copper ion concentration on the sensing performance of the sensor, the admittance measurements of 50 mM NaCl solutions with different copper ion concentrations were conducted, and the results in Figure 5d indicate that the change in copper ion concentration within sweat level has no significant effect on electrode admittance measurement, which benefits from a very low excitation voltage amplitude (0.2 V) and high excitation frequency (100 kHz) providing only weak drive force and short time for the electrochemical behavior of the

copper ion. Besides, the copper ion level in sweat is very low (5–20 μM); therefore, very weak electrochemical behavior exists. Then, the calibration area was tested in the solutions with different types of cations but the same concentration of chloride ion, and the results in Figure 5e reveal that the major cations in sweat have no effect on the admittance-sensing performance of the calibration area. At last, five sensors in the same batch were used in the calibration test, and the results indicate that the sensor based on ultraviolet laser cutting has good reproducibility (Figure 5f).

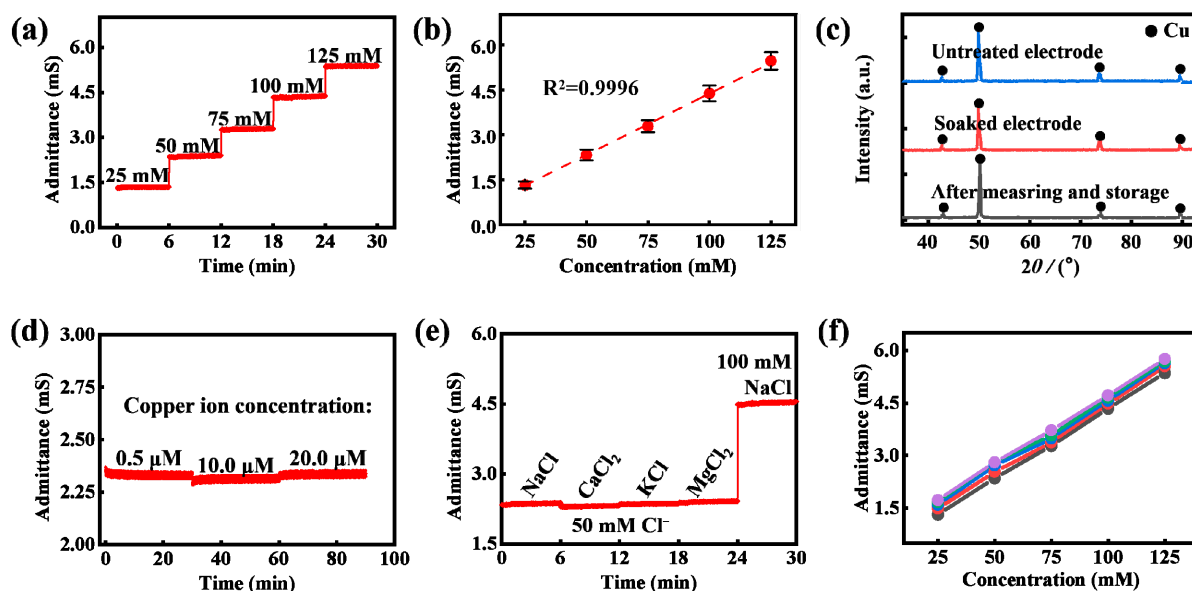


Figure 5. Sensing performance characterization of the calibration area. (a) Measured electrode admittances in NaCl solutions with different concentrations. (b) The calibration curve of the calibration area ($N = 5$), and the error bar represents standard deviation. (c) XRD characterization of copper electrodes. (d) Measured electrode admittances in 50 mM NaCl solutions with different copper ion concentrations (0.5, 10.0, and 20.0 μM). (e) Anti-interference performance of the calibration area. (f) Reproducibility of the sensor.

Notice that chloride ions and bicarbonates are most abundant ions in sweat, while the concentration of chloride ions is approximately 20 times greater than that of bicarbonates in sweat [32]. Other sweat anions are derived mainly from the ionization of weak acids, including uric acid, lactate and ascorbic acid. Their ionization constants are 5.1×10^{-6} , 1.4×10^{-4} and 5.0×10^{-5} , respectively. So the concentrations of corresponding anions in sweat are far less than the chloride ion concentration due to their very low ionization constants. Thus, sweat conductivity is approximately proportional to the chloride ion concentration, just like in previous reports [21,33,34]. Therefore, for the on-body trial, the measured electrode admittance in the calibration area can not only be used to calibrate the measured sweat rate from the detection area, but it can also be converted to the sweat Cl^- concentration, which is also a critical parameter for the assessment of electrolyte balance and the diagnosis of cystic fibrosis [35].

3.2. Characterizing the Sensing Performance of Detection Area for Sweat Rate Measurement

To characterize the sensing performance of the detection area for sweat rate measurement, we first injected 50 mM NaCl test solutions into the detection area with different injection rates, and the injections were paused for a period of time when the test solutions arrived at a certain site in microchannels. During the pause, electrode admittances remained constant, as illustrated at Platform I in Figure 6a. When the solutions completely filled the microchannels, the admittance values were also unchanged, as illustrated at Platform II in Figure 6a. The two platforms indicate that there was no zero drift of our sensors, implying that the copper electrode can be used for sweat admittance measurement (more detailed

analysis refers to Part I of the Supplementary Materials). Furthermore, the admittances of sweat with the same volume were approximately equal, as illustrated in Platform I and Platform II, demonstrating the reproducibility of the sensors. The change rates of the admittance with time in Figure 6a were proportional to injection rates (Figure 6b). This proportional relationship is consistent with Formula (2). As the experiments were conducted under the same rate, we could deduce the coefficient K in Formula (2), namely $K = 50 \text{ mM}/k' = 84.5 \text{ mM} \cdot \mu\text{L} \cdot \text{mS}^{-1}$, where k' is the slope of the fit curve in Figure 6b. Then we could obtain the measured flow rate according to Formula (2), as shown in Figure 6c and Figure S3. Then NaCl solutions with different concentrations were injected under the same rate, and the measured admittance changes are shown in Figure 6d. The admittance is approximately proportional to the solution concentration (Figure 6e), which validates the correctness of Formula (2). Figure 6f and Figure S4 show the measured sweat rates under different solution concentrations according to Formula (2). The experimental results indicate that the detection area combined with the calibration area is capable of accurately measuring the sweat rate.

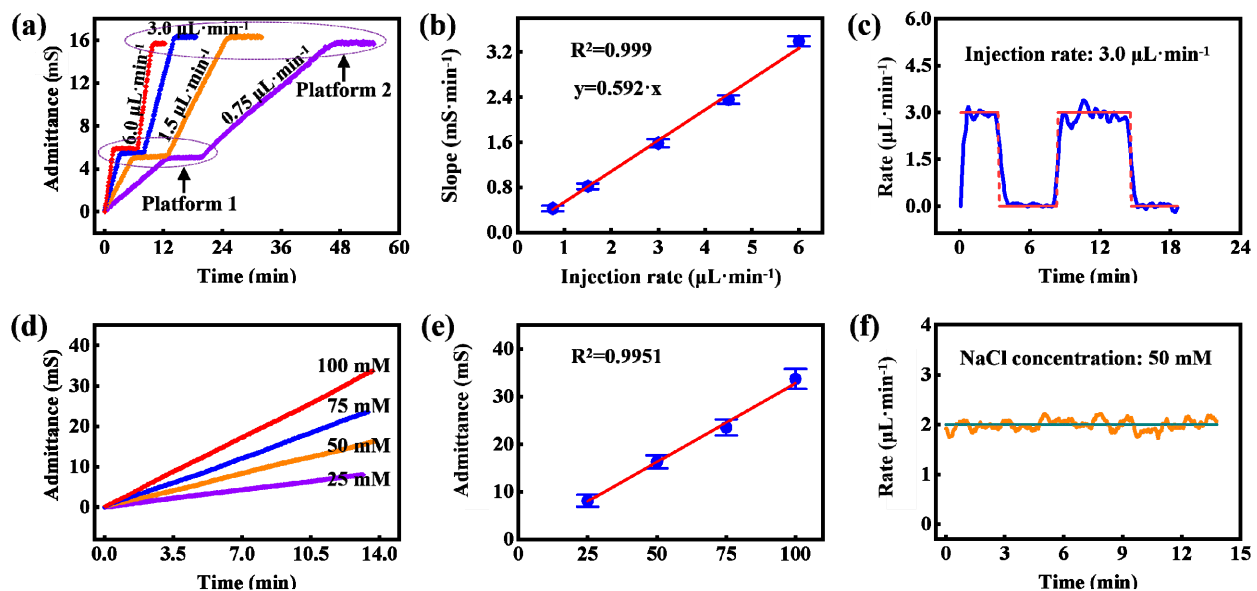


Figure 6. Characterizing the sensing performance of the detection area. (a) Measured electrode admittances under different injection rates but the same concentration of test solution. (b) The calibration curve between injection rate and the slope of increased admittance ($N = 5$), and the error bar represents standard deviation. (c) Measured flow rate at an injection rate of 3 $\mu\text{L} \cdot \text{min}^{-1}$. (d) Measured electrode admittances under different concentrations of test solutions but the same injection rate. (e) The calibration curve between injection rate and electrode admittance when microchannel was filled with test solution ($N = 5$), and the error bar represents standard deviation. (f) Measured flow rate under 50 mM NaCl solution at the injection rate of 2 $\mu\text{L} \cdot \text{min}^{-1}$.

As the copper electrode is utilized and the sweat copper-ion concentration ranges from 0.5 to 20 μM [32,36,37], it is necessary to investigate the influence of the copper ion concentration within sweat on the measurement result. Three 50 mM NaCl solutions containing different concentrations of copper ions were injected into the detection area, and the injections were paused at the same site of the microchannel for the same time. The results are displayed in Figure 7. The three curves almost overlap, which not only indicates the change in copper ion concentration within sweat has a negligible impact on electrode admittance measurement, but it also demonstrates the reproducibility of the sensor.

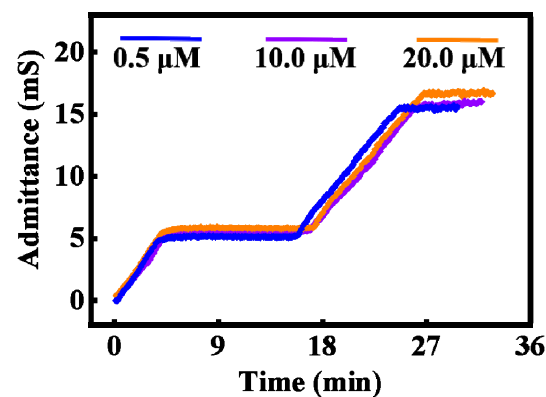


Figure 7. Measured electrode admittances of the detection area under 50 mM NaCl solutions with different copper ion concentrations (0.5, 10.0 and 20.0 μM) at the same injection rate.

3.3. On-Body Trial of the Sweat Rate via the Microfluidic Patch

In on-body trial, the trials were conducted on three subjects (subject I, subject II, and subject III). The verification of the measurement accuracy of the sweat-rate sensor was conducted on the forearm of subject I and the chest of subject II, and the regional variations in sweat rate at different parts of the body was also studied on the chest, back, forearm, and forehead of subject III. All subjects had been given informed consent before the trials. Sweat induction was implemented by exposure to high temperatures for subject I and subject II and being exposed to high temperature and performing stationary biking for subject III. The real-time electrode admittances of the calibration area and the detection area were measured and saved by the FPCB (Figure 8a). Image-based sweat-rate measurement was used to verify the validity of the on-body sweat-rate measurement of the microfluidic patch during the trials of subject I and subject II. In details, the real sweat volume in the microchannel was acquired by recording the optical image of the dyed sweat. The sweat rate calculated from the change rate of image-based sweat volume can be used as a reference to assess the accuracy of the microfluidic sweat sensor, as in previously reported studies [5,14,16,38]. To highlight the captured sweat in the microchannel, a high-concentration dye solution (sudan red solution) was dropped into the collection area of the microfluidic patch before the patch adhered to the skin, then the water in solution was evaporated and only the Sudan red dye was left at the collection area [39]. During the sweat-collection trial, the dye will be redissolved and turn the sweat red in color. The optical images of the sweat in the microchannel are shown in Figure 8b for subject I and Figure S5 for subject II.

During the trial on the forearm of subject I, sweat filled the calibration area at 23.5 min, then the electrode admittance of this area could output the available sensing signal for the quantification of the equivalent chloride ion concentration. The chloride ion concentration measured from the calibration area is shown in Figure 8c, and it underwent a process of increasing and then decreasing during the whole trial. Sweat entered the detection area at 27.1 min, then the electrode admittance of this area was valid. For the trial on the chest of subject II, the measured chloride ion concentration is shown in Figure 8e, which increased slightly during the trial process. The sweat rate was calculated from the electrode admittance of the detection area and the measured sweat chloride ion concentration, according to Formula (2), and the result with the unit of $\mu\text{L} \cdot \text{min}^{-1} \cdot \text{cm}^{-2}$ is shown as the solid red line in Figure 8d,f for the two subjects when the sweat-collection area is considered. Besides, the referenced sweat rate could be obtained from the optical images of the dyed sweat, as the blue dots in Figure 8d,f. The measured sweat rate from the admittance-based method is consistent with the referenced one, demonstrating the validity of the on-body measurement of the proposed sweat-rate sensor.

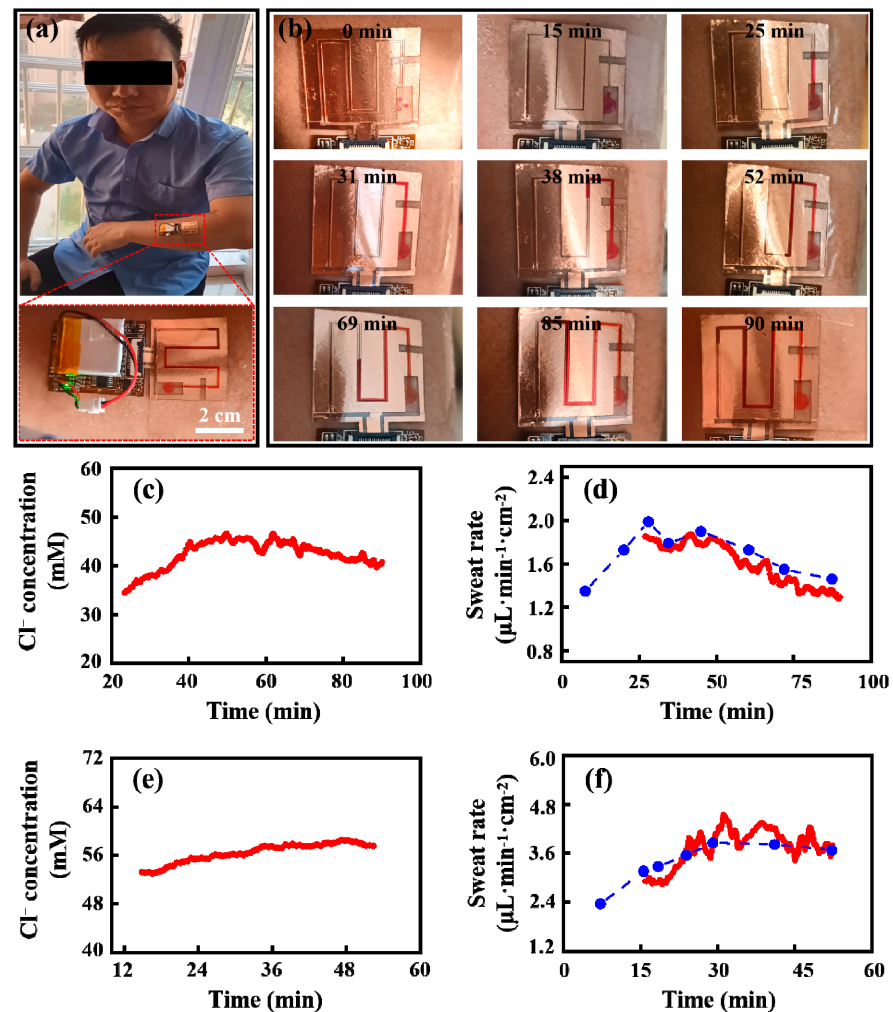


Figure 8. Results of on-body trial. (a) Depiction of on-body microfluidic patch and FPCB configuration mounted on the forearm of subject I during trial. (b) Photographs of sweat advancing in the microfluidic patch and corresponding time required to fill microchannel during the trial of subject I. (c) Measured sweat chloride ion concentration on the forearm of subject I from the admittance of the calibration area. (d) Measured sweat rate on the forearm of subject I from the admittance-based method and from the image-based method. (e) Measured sweat chloride ion concentration on the chest of subject II from the admittance of the calibration area. (f) Measured sweat rate on the chest of subject II from the admittance-based method and from the image-based method.

From the referenced sweat rate, it can be found that sweat rate increased for a period of time after the onset of sweat induction, probably due to delayed perspiration from external stimuli. This trend is analogous to previously reported studies using other measuring approaches [13,14]. The change trend in the sweat rate is similar to that of the chloride ion, implying some correlations between the sweat chloride ion concentration and the sweat rate, which is consistent with previously reported studies [5,16,17]. This consistency may be because there is more time to reabsorb chloride ions with a low sweat rate and less time with a high sweat rate in the gland during the sweat secretion process [32].

In trials of different parts of the body of subject III, except for the forearm, all trials ended when the microchannels were filled. The results are illustrated in Figure 9. The sweat rate on his forearm is the lowest, while that on his chest is the highest. On the chest, the sweat rate almost stayed constant during the whole trial process, but on the other three parts, it declined especially in the second half of the trials. Comparing the results of the four parts, the sweat chloride ion concentrations were more concentrated at higher sweat rates, which is consistent with previous studies [17,40]. Furthermore,

the change trend in sweat chloride ion is similar to that of the sweat rate. This trend is similar to previous reports [17,20], which may be due to the secretion rate of chloride ion in secretory coil of sweat glands increasing proportionally with the sweat rate, but it is larger than the reabsorption rate in the proximal duct of sweat glands, so that a higher final concentration of chloride ions is obtained at a greater sweat rate when sweat arrives at the skin surface [41].

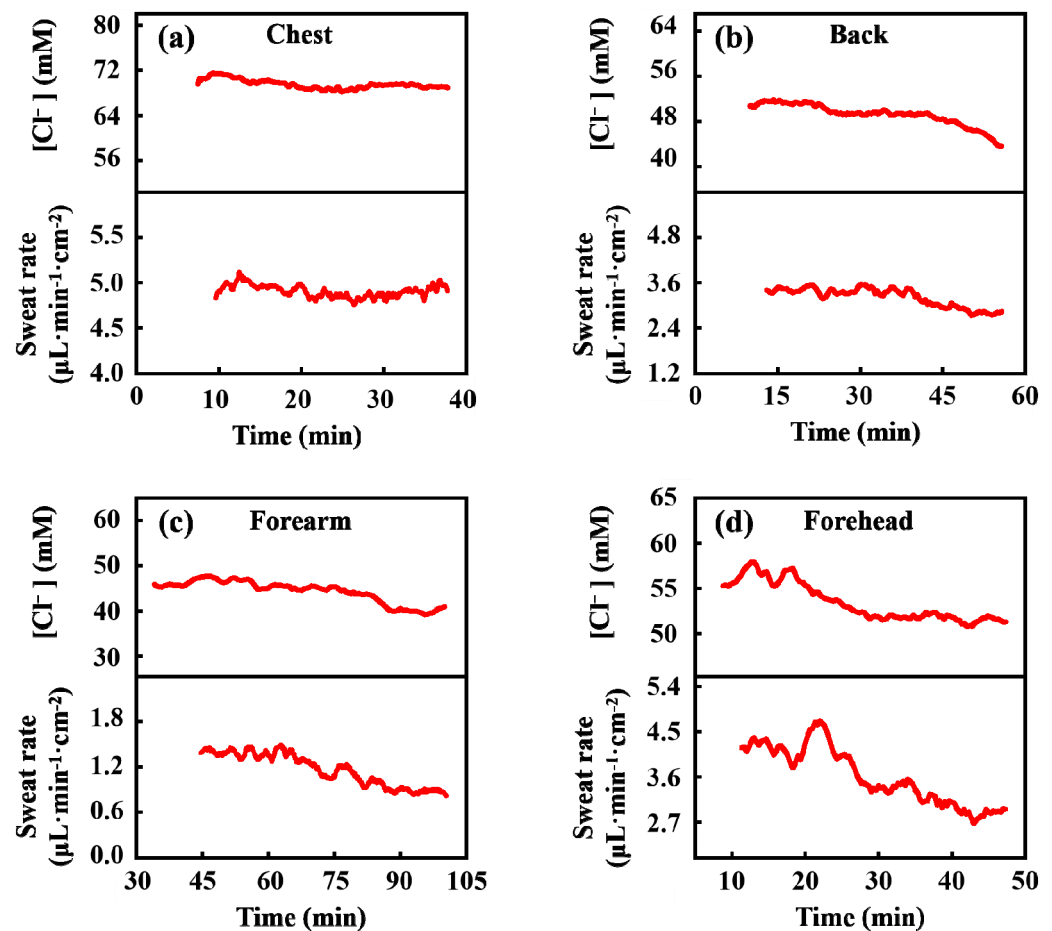


Figure 9. Regional sweat rate and chloride concentration at chest (a), back (b), forearm (c), and forehead (d) of Subject III, respectively.

Because the valid electrode admittance measured by FPCB only starts from sweat filling the calibration area or entering the detection area, there are delays for the measurements of sweat chloride ions and the sweat rate. Future studies should focus on the optimization of the structure of the microfluidic patch to reduce detection delay. Besides, the effective detection time of the sweat rate is limited by the volume of the microchannel. Notice that most studies indicate that the range of the sweat rate is generally ranges within 0.5 to 20 $\mu L \cdot min^{-1} \cdot cm^{-2}$ [5,9,12,13,15,16,42,43], as illustrated in Table S1. As the volume of the detection area is 22 μL , the effective detection time of the sweat-rate sensor approximately ranges from 5.5 min to 224.5 min for a 5 mm-diameter sweat-collection area in this work. The detection time can be extended by increasing the channel length or channel height so as to increase the volume of the microchannel.

4. Conclusions

To sum up, we proposed a simple, low-cost and easy-to-manufacture microfluidic patch for admittance-based sweat-rate sensing. This patch can be rapidly manufactured by only laser-cutting and transfer-printing, free of any surface treatment or modification of the electrodes and without alignment operation. A copper electrode made of copper

foil tape was used for the measurement of the sweat rate. We successfully solved the potential interference problems of the copper electrode in admittance-based sweat-sensing by filtering the DC component of the excitation signal of the sensor and optimizing the frequency and amplitude of the signal. Compared with previously published studies, the copper electrode is capable of achieving the same performance as the gold electrode in the admittance-based measurement of sweat electrolyte concentration [17] and sweat rate [16]. However, under the condition of the same sensing performance, the proposed full-cut manufacture and design scheme can provide an easy-to-manufacture and low-cost path to fabricate a skin-interfaced sweat-rate sensor. Future studies will focus on improving the flexible circuits to enable wireless transmitting the measured data to mobile devices and optimizing the sensor structure to reduce detection delay.

Supplementary Materials: The following supporting information can be downloaded at: <https://www.mdpi.com/article/10.3390/bios13010067/s1>, PART I: The feasibility of copper electrode for admittance-based sensing of sweat rate [32,36,37]; PART II: Formula derivation of sweat rate [44]; PART III: Derivation process of the flow resistance of microchannel [7,45–47]; Part IV: Figure and table supplementary for detailing the design and characterization of the proposed microfluidic sweat-rate sensor; Figure S1: Layout of electrodes and centerline-gap in microchannel; Figure S2: Photograph of the in vitro flow injection test system; Figure S3: Measured flow rate at injection rate of 0.75, 1.5 and 6.0 $\mu\text{L}\cdot\text{min}^{-1}$, respectively; Figure S4: Measured flow rate at the same injection rate of 2.0 $\mu\text{L}\cdot\text{min}^{-1}$ under three test solutions with different NaCl concentrations; Figure S5: Photographs of sweat advancing in the microfluidic patch and corresponding time required to fill microchannel during the trial of subject II; Figure S6: EIS Nyquist plot of the electrodes in calibration area in different concentrations of chloride ion solutions; Table S1: The sweat rates in previously reported works.

Author Contributions: Conceptualization, L.W. and A.L.; methodology, L.W.; software, L.W. and Y.H.; validation, Z.L., H.W. and A.L.; formal analysis, L.W., Y.H., D.G. and L.C.; investigation, L.W. and Y.H.; resources, L.W., H.W. and A.L.; data curation, L.W. and Y.H.; writing—original draft preparation, L.W.; writing—review and editing, L.W., Y.H. and A.L.; visualization, L.W. and Y.H.; supervision, A.L.; project administration, L.W. and A.L.; funding acquisition, A.L., L.W. and Y.H. contribute equally to this work. All authors have read and agreed to the published version of the manuscript.

Funding: This work was supported by the Zhejiang Provincial Natural Science Foundation of China (Nos. LR19E020004 and LR20A020002), the Youth Top-notch Talent Project of Zhejiang Ten Thousand Plan of China (No. ZJWR0308010) and the National Natural Science Foundation of China (Nos. 12272351, 11672269 and 11972323).

Institutional Review Board Statement: Not applicable.

Informed Consent Statement: Not applicable.

Data Availability Statement: All relevant data is included in the manuscript and Supplementary Materials.

Conflicts of Interest: The authors declare no conflict of interest.

References

1. Kraft, J.A.; Green, J.M.; Bishop, P.A.; Richardson, M.T.; Neggers, Y.H.; Leeper, J.D. The influence of hydration on anaerobic performance: A review. *Res. Q. Exerc. Sport* **2012**, *83*, 282–292. [[CrossRef](#)] [[PubMed](#)]
2. Nuccio, R.P.; Barnes, K.A.; Carter, J.M.; Baker, L.B. Fluid balance in team sport athletes and the effect of hypohydration on cognitive, technical, and physical performance. *Sports Med.* **2017**, *47*, 1951–1982. [[CrossRef](#)] [[PubMed](#)]
3. McDermott, B.P.; Anderson, S.A.; Armstrong, L.E.; Casa, D.J.; Chevront, S.N.; Cooper, L.; Kenney, W.L.; O'Connor, F.G.; Roberts, W.O. National athletic trainers' association position statement: Fluid replacement for the physically active. *J. Athl. Train.* **2017**, *52*, 877–895. [[CrossRef](#)] [[PubMed](#)]
4. Montain, S.J.; Chevront, S.N.; Sawka, M.N. Exercise associated hyponatraemia: Quantitative analysis to understand the aetiology. *Br. J. Sports Med.* **2006**, *40*, 98–105. [[CrossRef](#)]
5. Baker, L.B.; Model, J.B.; Barnes, K.A.; Anderson, M.L.; Lee, S.P.; Lee, K.A.; Brown, S.D.; Reimel, A.J.; Roberts, T.J.; Nuccio, R.P.; et al. Skin-interfaced microfluidic system with personalized sweating rate and sweat chloride analytics for sports science applications. *Sci. Adv.* **2020**, *6*, eabe3929. [[CrossRef](#)]

6. Choi, J.; Chen, S.; Deng, Y.; Xue, Y.; Reeder, J.T.; Franklin, D.; Oh, Y.S.; Model, J.B.; Aranyosi, A.J.; Lee, S.P.; et al. Skin-interfaced microfluidic systems that combine hard and soft materials for demanding applications in sweat capture and analysis. *Adv. Healthc. Mater.* **2020**, *10*, 2000722. [\[CrossRef\]](#)
7. Reeder, J.T.; Choi, J.; Xue, Y.; Gutruf, P.; Hanson, J.; Liu, M.; Ray, T.; Bandodkar, A.J.; Avila, R.; Xia, W.; et al. Waterproof, electronics-enabled, epidermal microfluidic devices for sweat collection, biomarker analysis, and thermography in aquatic settings. *Sci. Adv.* **2019**, *5*, eaau6356. [\[CrossRef\]](#)
8. Bandodkar, A.J.; Gutruf, P.; Choi, J.; Lee, K.; Sekine, Y.; Reeder, J.T.; Jeang, W.J.; Aranyosi, A.J.; Lee, S.P.; Model, J.B.; et al. Battery-free, skin-interfaced microfluidic/electronic systems for simultaneous electrochemical, colorimetric, and volumetric analysis of sweat. *Sci. Adv.* **2019**, *5*, eaav3294. [\[CrossRef\]](#)
9. Koh, A.; Kang, D.; Xue, Y.; Lee, S.; Pielak, R.M.; Kim, J.; Hwang, T.; Min, S.; Banks, A.; Bastien, P.; et al. A soft, wearable microfluidic device for the capture, storage, and colorimetric sensing of sweat. *Sci. Transl. Med.* **2016**, *8*, 366ra165. [\[CrossRef\]](#)
10. Shi, H.H.; Cao, Y.; Zeng, Y.; Zhou, Y.; Wen, W.; Zhang, C.; Zhao, Y.; Chen, Z. Wearable tesla valve-based sweat collection device for sweat colorimetric analysis. *Talanta* **2022**, *240*, 123208. [\[CrossRef\]](#)
11. Zhao, F.J.; Bonmarin, M.; Chen, Z.C.; Larson, M.; Fay, D.; Runnoe, D.; Heikenfeld, J. Ultra-simple wearable local sweat volume monitoring patch based on swellable hydrogels. *Lab Chip* **2020**, *20*, 168–174. [\[CrossRef\]](#)
12. Wang, L.; Xu, T.; Fan, C.; Zhang, X. Wearable strain sensor for real-time sweat volume monitoring. *iScience* **2021**, *24*, 102028. [\[CrossRef\]](#)
13. Kwon, K.; Kim, J.U.; Deng, Y.; Krishnan, S.R.; Choi, J.; Jang, H.; Lee, K.; Su, C.-J.; Yoo, I.; Wu, Y.; et al. An on-skin platform for wireless monitoring of flow rate, cumulative loss and temperature of sweat in real time. *Nat. Electron.* **2021**, *4*, 302–312. [\[CrossRef\]](#)
14. Choi, D.-H.; Gonzales, M.; Kitchen, G.B.; Phan, D.-T.; Searson, P.C. A capacitive sweat rate sensor for continuous and real-time monitoring of sweat loss. *ACS Sens.* **2020**, *5*, 3821–3826. [\[CrossRef\]](#)
15. Hourlier-Fargette, A.; Schon, S.; Xue, Y.; Avila, R.; Li, W.; Gao, Y.; Liu, C.; Kim, S.B.; Raj, M.S.; Fields, K.B.; et al. Skin-interfaced soft microfluidic systems with modular and reusable electronics for in situ capacitive sensing of sweat loss, rate and conductivity. *Lab Chip* **2020**, *20*, 4391–4403. [\[CrossRef\]](#)
16. Nyein, H.Y.Y.; Tai, L.C.; Ngo, Q.P.; Chao, M.; Zhang, G.B.; Gao, W.; Bariya, M.; Bullock, J.; Kim, H.; Fahad, H.M.; et al. A wearable microfluidic sensing patch for dynamic sweat secretion analysis. *ACS Sens.* **2018**, *3*, 944–952. [\[CrossRef\]](#)
17. Kim, S.B.; Lee, K.; Raj, M.S.; Lee, B.; Reeder, J.T.; Koo, J.; Hourlier-Fargette, A.; Bandodkar, A.J.; Won, S.M.; Sekine, Y.; et al. Soft, skin-interfaced microfluidic systems with wireless, battery-free electronics for digital, real-time tracking of sweat loss and electrolyte composition. *Small* **2018**, *14*, 1802876. [\[CrossRef\]](#)
18. Nyein, H.Y.Y.; Bariya, M.; Kivimäki, L.; Uusitalo, S.; Liaw, T.S.; Jansson, E.; Ahn, C.H.; Hangasky, J.A.; Zhao, J.; Lin, Y.; et al. Regional and correlative sweat analysis using high-throughput microfluidic sensing patches toward decoding sweat. *Sci. Adv.* **2019**, *5*, eaaw9906. [\[CrossRef\]](#)
19. Francis, J.; Stamper, I.; Heikenfeld, J.; Gomez, E.F. Digital nanoliter to milliliter flow rate sensor with in vivo demonstration for continuous sweat rate measurement. *Lab Chip* **2019**, *19*, 178–185. [\[CrossRef\]](#)
20. Yuan, Z.; Hou, L.; Bariya, M.; Nyein, H.Y.Y.; Tai, L.-C.; Ji, W.; Li, L.; Javey, A. A multi-modal sweat sensing patch for cross-verification of sweat rate, total ionic charge, and Na⁺ concentration. *Lab Chip* **2019**, *19*, 3179–3189. [\[CrossRef\]](#)
21. Steijlen, A.S.M.; Jansen, K.M.B.; Bastemeijer, J.; French, P.J.; Bossche, A. Low-cost wearable fluidic sweat collection patch for continuous analyte monitoring and off-line analysis. *Anal. Chem.* **2022**, *94*, 6893–6901.
22. Yang, Q.; Rosati, G.; Abarintos, V.; Aroca, M.A.; Osmá, J.F.; Merkoçi, A. Wearable and fully printed microfluidic nanosensor for sweat rate, conductivity, and copper detection with healthcare applications. *Biosens. Bioelectron.* **2022**, *202*, 114005. [\[CrossRef\]](#) [\[PubMed\]](#)
23. Masud, J.; Liyanage, W.P.R.; Cao, X.; Saxena, A.; Nath, M. Copper selenides as high-efficiency electrocatalysts for oxygen evolution reaction. *ACS Appl. Energy Mater.* **2018**, *1*, 4075–4083. [\[CrossRef\]](#)
24. Saxena, A.; Liyanage, W.; Masud, J.; Kapila, S.; Nath, M. Selective electroreduction of CO₂ to carbon-rich products with a simple binary copper selenide electrocatalyst. *J. Mater. Chem. A* **2021**, *9*, 7150–7161. [\[CrossRef\]](#)
25. Wang, Z.H.; Gong, L.K.; Zeng, H.; Yang, T.; Luo, X.L. A novel ratiometric electrochemical cupric ion sensing strategy based on unmodified electrode. *Anal. Chim. Acta* **2021**, *1146*, 11–16. [\[CrossRef\]](#)
26. Sonner, Z.; Wilder, E.; Heikenfeld, J.; Kasting, G.; Beyette, F.; Swaile, D.; Sherman, F.; Joyce, J.; Hagen, J.; Loughnane, N.K.; et al. The microfluidics of the eccrine sweat gland, including biomarker partitioning, transport, and biosensing implications. *Biomicrofluidics* **2015**, *9*, 031301. [\[CrossRef\]](#)
27. Zhong, B.; Jiang, K.; Wang, L.; Shen, G. Wearable sweat loss measuring devices: From the role of sweat loss to advanced mechanisms and designs. *Adv. Sci.* **2022**, *9*, 2103257. [\[CrossRef\]](#)
28. Zhang, X.; Liu, H.; Yue, L.; Bai, Y.; He, J. Fabrication of acrylic pressure-sensitive adhesives containing maleimide for heat-resistant adhesive applications. *Polym. Bull.* **2019**, *76*, 3093. [\[CrossRef\]](#)
29. El-Saftawy, A.A.; Elfalaky, A.; Ragheb, M.S.; Zakhary, S.G. Electron beam induced surface modifications of PET film. *Radiat. Phys. Chem.* **2014**, *102*, 96. [\[CrossRef\]](#)
30. Yang, S.; Chen, Y.C.; Nicolini, L.; Pasupathy, P.; Lu, N. “Cut-and-paste” manufacture of multi-parametric epidermal sensor systems. *Adv. Mater.* **2015**, *27*, 6423–6430. [\[CrossRef\]](#)

31. Jeong, H.; Wang, L.; Ha, T.; Mitbender, R.; Yang, X.; Dai, Z.; Qiao, S.; Shen, L.; Sun, N.; Lu, N. Modular and reconfigurable wireless e-tattoos for personalized sensing. *Adv. Mater. Technol.* **2019**, *4*, 1900117. [[CrossRef](#)]
32. Baker, L.B.; Wolfe, A.S. Physiological mechanisms determining eccrine sweat composition. *Eur. J. Appl. Physiol.* **2020**, *120*, 719–752. [[CrossRef](#)]
33. Mattar, A.C.V.; Leone, G.; Rodrigues, J.C.; Adde, F.V.J. Sweat conductivity: An accurate diagnostic test for cystic fibrosis? *J. Cyst. Fibros.* **2014**, *13*, 528. [[CrossRef](#)]
34. Domingos, M.T.; Magdalena, N.I.R.; Cat, M.N.L.; Watanabe, A.M.; Filho, N.A.R. Sweat conductivity and coulometric quantitative test in neonatal cystic fibrosis screening condutividade e teste quantitativo coulométrico na triagem neonatal para fibrose cística. *J. Pediatr.* **2015**, *91*, 590. [[CrossRef](#)]
35. Hauke, A.; Oertel, S.; Knoke, L.; Fein, V.; Maier, C.; Brinkmann, F.; Jank, M.P.M. Screen-printed sensor for low-cost chloride analysis in sweat for rapid diagnosis and monitoring of cystic fibrosis. *Biosensors* **2020**, *10*, 123. [[CrossRef](#)]
36. Bagheri, N.; Mazzaracchio, V.; Cinti, S.; Colozza, N.; Natale, C.D.; Netti, P.A.; Saraji, M.; Roggero, S.; Moscone, D.; Arduini, F. Electroanalytical sensor based on gold nanoparticle decorated paper for sensitive detection of copper ions in sweat and serum. *Anal. Chem.* **2021**, *93*, 5225–5233. [[CrossRef](#)]
37. Gao, W.; Nyein, H.Y.Y.; Shahpar, Z.; Fahad, H.M.; Chen, K.; Emaminejad, S.; Gao, Y.; Tai, L.C.; Wu, H.E.; Bullock, J.; et al. Wearable microsensor array for multiplexed heavy metal monitoring of body fluids. *ACS Sens.* **2016**, *1*, 866–874. [[CrossRef](#)]
38. Brueck, A.; Iftekhhar, T.; Stannard, A.B.; Yelamarthi, K.; Kaya, T. A real-time wireless sweat rate measurement system for physical activity monitoring. *Sensors* **2018**, *18*, 533. [[CrossRef](#)]
39. Wei, L.; Fang, G.; Kuang, Z.; Cheng, L.; Wu, H.; Guo, D.; Liu, A. 3D-printed low-cost fabrication and facile integration of flexible epidermal microfluidics platform. *Sens. Actuators B Chem.* **2022**, *353*, 131085. [[CrossRef](#)]
40. Baker, L.B.; Ungaro, C.T.; Sopeña, B.C.; Nuccio, R.P.; Reimel, A.J.; Carter, J.M.; Stofan, J.R.; Barnes, K.A. Body map of regional vs whole body sweating rate and sweat electrolyte concentrations in men and women during moderate exercise-heat stress. *J. Appl. Physiol.* **2018**, *124*, 1304–1318. [[CrossRef](#)]
41. Baker, L.B. Sweating rate and sweat sodium concentration in athletes: A review of methodology and intra/interindividual variability. *Sports Med.* **2017**, *47* (Suppl. 1), S111–S128. [[CrossRef](#)] [[PubMed](#)]
42. Wang, L.; Lu, J.; Li, Q.; Li, L.; He, E.; Jiao, Y.; Ye, T.; Zhang, Y. A core-sheath sensing yarn-based electrochemical fabric system for powerful sweat capture and stable sensing. *Adv. Funct. Mater.* **2022**, *32*, 2200922. [[CrossRef](#)]
43. Kim, S.; Park, S.; Choi, J.; Hwang, W.; Kim, S.; Choi, I.-S.; Yi, H.; Kwak, R. An epifluidic electronic patch with spiking sweat clearance for event-driven perspiration monitoring. *Nat. Commun.* **2022**, *13*, 6705. [[CrossRef](#)] [[PubMed](#)]
44. Randviir, E.P.; Banks, C.E. Electrochemical impedance spectroscopy: An overview of bioanalytical applications. *Anal. Methods* **2013**, *5*, 1098–1115. [[CrossRef](#)]
45. Delamarche, E.; Bernard, A.; Schmid, H.; Bietsch, A.; Michel, B.; Biebuyck, H. Microfluidic networks for chemical patterning of substrates: Design and application to bioassays. *J. Am. Chem. Soc.* **1998**, *120*, 500–508. [[CrossRef](#)]
46. Choi, J.; Kang, D.; Han, S.; Kim, S.B.; Rogers, J.A. Thin, soft, skin-mounted microfluidic networks with capillary bursting valves for chrono-sampling of sweat. *Adv. Healthc. Mater.* **2017**, *6*, 1601355. [[CrossRef](#)]
47. Ladosz, A.; von Rohr, P.R. Design rules for microscale capillary phase separators. *Microfluid. Nanofluid.* **2017**, *21*, 153. [[CrossRef](#)]

Disclaimer/Publisher’s Note: The statements, opinions and data contained in all publications are solely those of the individual author(s) and contributor(s) and not of MDPI and/or the editor(s). MDPI and/or the editor(s) disclaim responsibility for any injury to people or property resulting from any ideas, methods, instructions or products referred to in the content.